I&EC research
Industrial & Engineering Chemistry Research

Research Note

pubs.acs.org/IECR

Particle Image Velocimetry (PIV) Investigation of Flow Characteristics in Confined Impinging Jet Reactors

Zhengming Gao, Jing Han, Yingdao Xu, Yuyun Bao, and Zhipeng Li*

State Key Laboratory of Chemical Resource Engineering, School of Chemical Engineering, Beijing University of Chemical Technology, Mailbox 230, Beijing 100029, People's Republic of China

ABSTRACT: The flow characteristics in confined impinging jet reactors (CIJRs) were investigated, using particle image velocimetry. The effects of Reynolds number (Re), jet velocity ratio (u_1/u_2), jet diameter (d), and the factor L (defined as the distance between the axes of two jets and the top wall of the CIJR chamber) on the flow characteristics of CIJRs were discussed. The similarity of the turbulent flow in CIJRs was extended to the operating conditions with high Reynolds numbers, ranging from Re = 10 620 to Re = 21 210. The position of the stagnation point in CIJR is closely related to u_1/u_2, but independent of d. The decrease of the ratio of the factor L to impinging jet diameter (L/d) from 4 to 1.5 can increase the values of turbulent kinetic energy and intensify momentum transfer and mixing in the impinging region of CIJR. The present study shows that CIJRs are ideal reactors for rapid chemical reactions, and optimized parameters are helpful for the design and operation of such reactors.

1. INTRODUCTION

Confined impinging jet reactors (CIJRs) are widely used in various process industries, such as absorption and desorption,[1] drying,[2] extraction,[3] mixing,[4−7] bioreaction,[8] crystallization,[9] and precipitation.[10] The principle of CIJRs is to make at least two impinging jets collide with each other and intensify the momentum, heat, and mass transfer in the impinging region. Therefore, CIJRs offer many advantages for rapid chemical processes. In recent years, there has been a renewed interest in these devices, because they can achieve good mixing much faster than other reactors such as stirred tanks. Several mixing studies of CIJRs have been published over the past decades. Johnson and Prud'homme[11] performed a micromixing study on a second-order parallel dimethoxypropane (DMP) reaction and discussed the effect of reactor geometry and operating conditions on the micromixing. Liu and Fox[12] used a computational fluid dynamics (CFD) model for computational studies of micromixing with a DMP reaction in the CIJR with impinging diameters of 0.5 mm. Gavi et al.[13] studied the mixing and reaction in CIJRs by means of CFD method. Siddiqui et al.[14] investigated the energy dissipation rate and mixing efficiency of CIJRs with low Reynolds number (Re) values, using iodide−iodate reactions.

A few studies have focused on the flow characteristics in CIJRs. Liu et al.[15] employed microscopic particle image velocimetry (microPIV) techniques and CFD procedures to study a planar microscale CIJR with Re values in the range of 211−1003. Icardi et al.[16] investigated the flow fields in a CIJR with four inlet flow rates, using microPIV and direct numerical simulation, presenting both the mean and the fluctuation velocity fields. However, the effect of geometric parameters and operating conditions, such as jet diameter, jet velocity ratio, and the distance between the axes of two jets and the top wall of CIJR chamber (L), on the flow characteristics of CIJRs has not been reported until the present work.

Motivated by the great potential of CIJRs and the need for understanding the flow characteristics in CIJRs to promote beneficial applications, we determined (1) the mean velocity and turbulent kinetic energy (TKE) distributions at high Reynolds numbers, (2) the relationship between the stagnation point and mean velocity ratio for impinging jets with different diameters, and (3) the effect of the factor L on TKE distribution.

2. EXPERIMENTAL SECTION

2.1. Experimental Setup. A schematic diagram of the experimental apparatus is shown in Figure 1. The apparatus

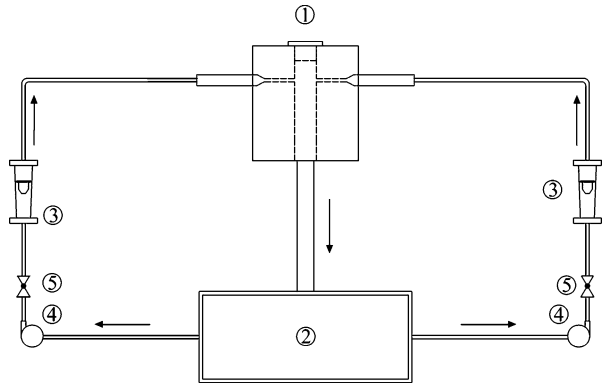

Figure 1. Experimental setup: (1) confined impinging jet reactor (CIJR), (2) storage tank, (3) rotameters, (4) centrifugal pumps, and (5) valves.

consists of five parts: (1) a CIJR made of copper and manufactured by using computer-controlled machine tools, (2) a storage tank made of acrylic for the circulation of deionized water, (3) two rotameters (LZB-15, Changzhou Qinfeng Flowmeter Corporation, China) to measure the flow rates of the two jets of

Received: March 21, 2013
Revised: June 22, 2013
Accepted: July 26, 2013
Published: July 26, 2013

   dx.doi.org/10.1021/ie400891u | *Ind. Eng. Chem. Res.* 2013, 52, 11779−11786

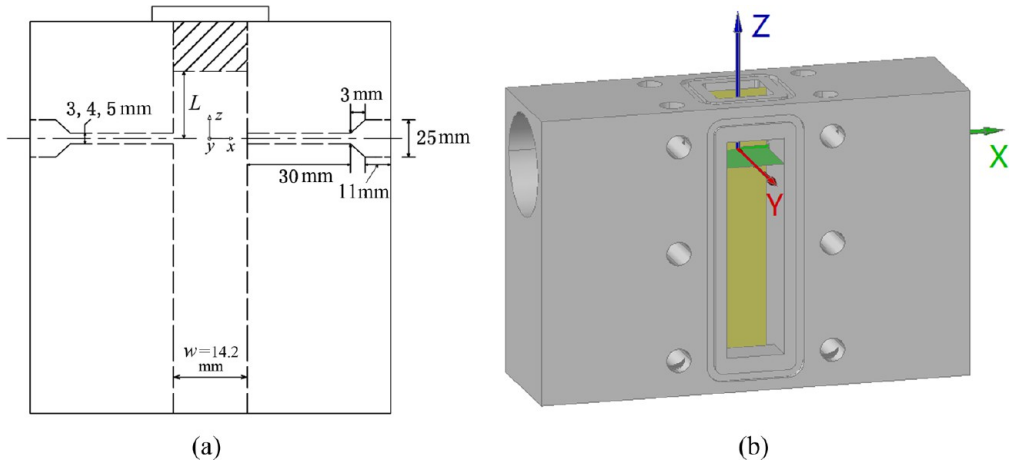

Figure 2. Dimensions and solid model of a CIJR (yellow: $x-z$ plane; green: $x-y$ plane).

Table 1. Operating Conditions for CIJRs

	d_1 (mm)	d_2 (mm)	u_1 (m/s)	u_2 (m/s)	Re_1	Re_2	L (mm)
Group 1	3	3	3.54−7.07	3.54−7.07	10 620−21 210	10 620−21 210	7.5
Group 2	3	3	7.86	7.07−8.65	23 580	21 210−25 950	7.5
	4	4	4.53	4.11−5.05	18 120	16 440−20 200	7.5
	5	5	3.52	3.23−3.87	17 600	16 150−19 350	7.5
Group 3	3	3	5.89	5.89	17 670	17 670	4.5−12

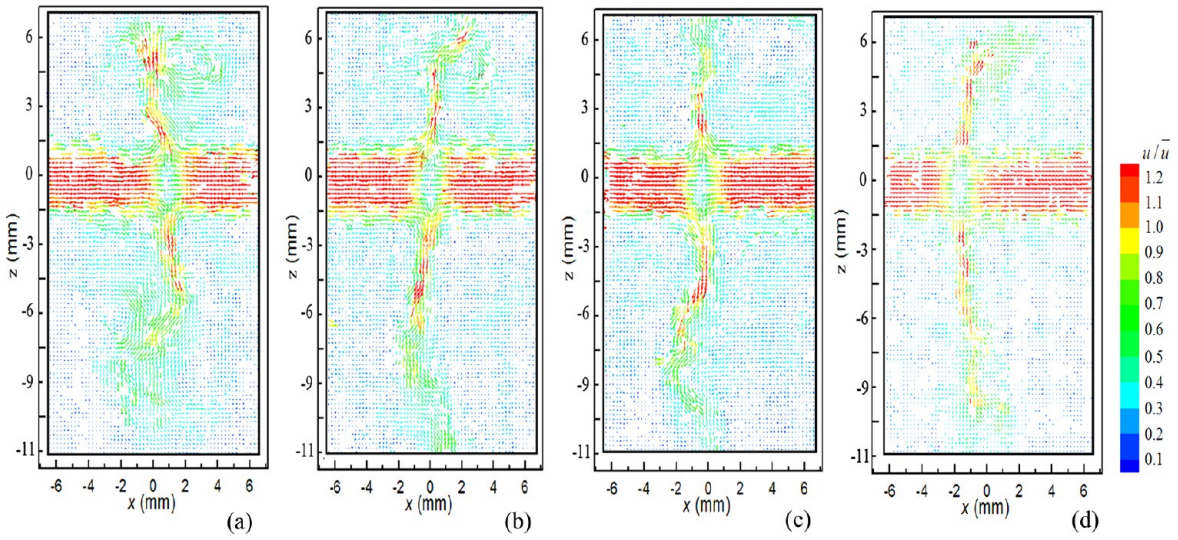

Figure 3. Instantaneous flow field on $x-z$ plane of CIJR at Re = 21 210.

the CIJR, (4) two centrifugal pumps (25FS, Beijing Beiguang Anticorrosive Equipment Corporation, China), and (5) two valves for controlling the flow ratio of the two jets. The chamber of the CIJR was sealed by transparent acrylic to provide convenient measurement regions for the particle image velocimetry (PIV) experiments. Figure 2 shows the dimensions and the solid model of the CIJR used.

2.2. PIV Technique and TKE Definition. The commercial two-dimensional (2D) PIV system (TSI, USA) used in the present study included a laser (New Wave Research Solo Nd:YAG, 200 mJ, 15 Hz), a camera (PowerView Plus, 4008 × 2672 pixels), a synchronizer, and Insight 3G software. The time difference between laser pulses, Δt, was optimized to ensure that the maximum in-plane and out-of-plane displacements of the particles were less than one-quarter of the sizes of the interrogation windows and the thickness of the lightsheet. Thus, Δt varied from 8 μs to 22 μs when the mean jet velocity was in the range of 8.65−3.23 m/s. The measured images were interrogated by 32 × 32 pixels windows with 50% overlap, and then instantaneous velocities were obtained by using a two-frame cross-correlation algorithm. The spatial resolution of the velocity vectors was ~0.21 mm. The statistic independency was verified on the mean and fluctuating velocities, and the difference between the fluctuating velocities calculated from 200 and 300 pairs of images was <2%. Thus, 300 pairs of images were captured for each experiment.

The experimental error caused by the particle image processing is ~1/10 of the seed particle image diameter.[17,18]

dx.doi.org/10.1021/ie400891u | Ind. Eng. Chem. Res. 2013, 52, 11779−11786

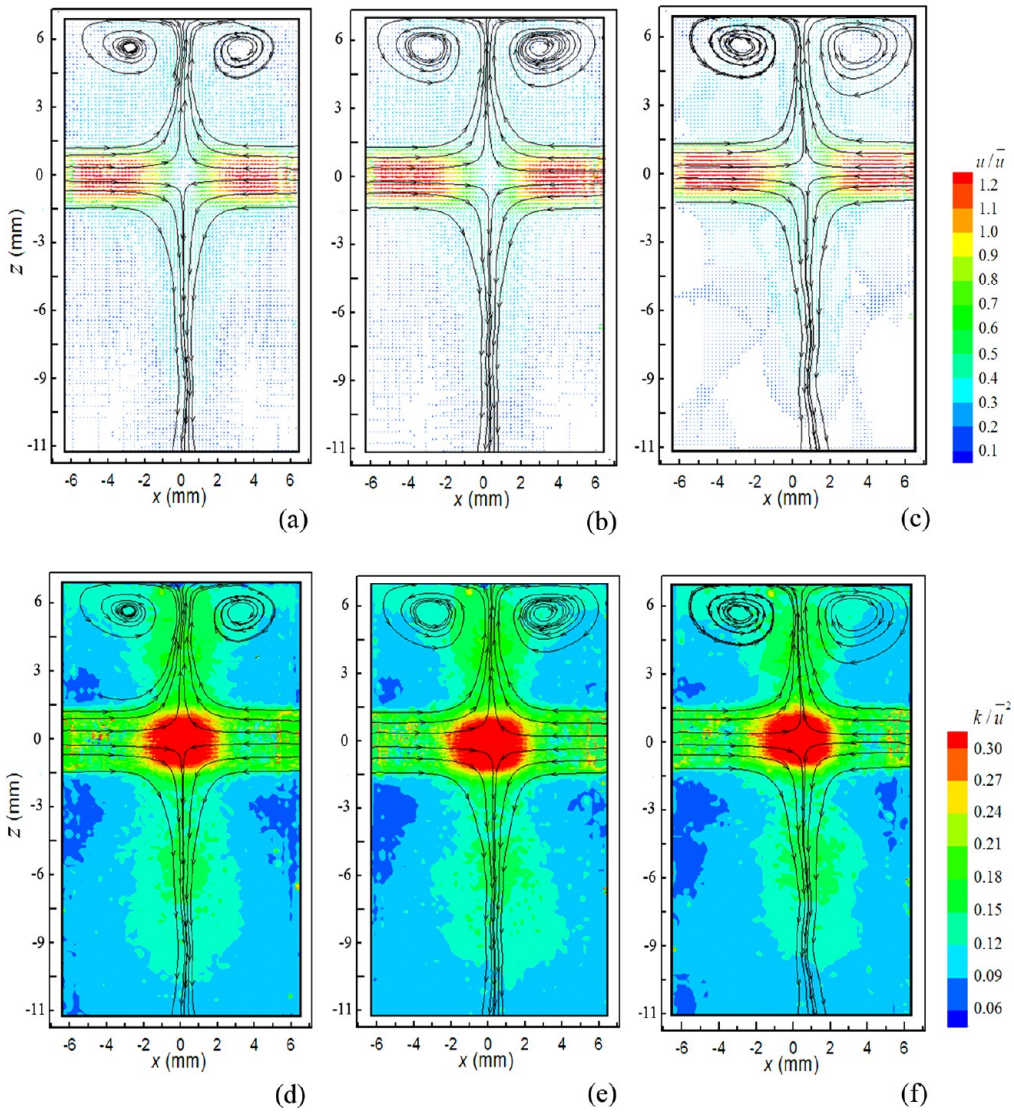

Figure 4. Normalized mean velocity and TKE distributions on $x-z$ plane of CIJR at ((a) and (d)) Re = 10 620, ((b) and (e)) Re = 14 150, and ((c) and (f)) Re = 21 210 (u_1/u_2 = 1.0).

In this study, the particle image diameter is ∼30 μm, and the effective particle diameter is ∼20 μm, as projected back to the flow coordinates. Thus, the experimental error of the particle displacements is within 2.0 μm. The particles travel ∼100 μm in every laser pulse, resulting in an experimental error of ∼2.0%.

Two orthogonal planes through the axes of the two jets—namely, the $x-y$ and $x-z$ planes shown in Figure 2b—were chosen as measurement planes to illustrate the flow characteristics in the CIJR. The dimensions of the $x-y$ plane are 14.2 mm × 14.2 mm, and those of the $x-z$ plane are 14.2 mm × ∼19.5 mm.

The mean velocities in the two jets u_i can be calculated from the corresponding volumetric flow rates Q_i:

$$u_i = \frac{Q_i}{(\pi/4)d_i^{\,2}} \tag{1}$$

where d_i is the inner diameter of the jet.

The Reynolds numbers in the two jets are defined as follows:

$$Re_i = \frac{d_i u_i}{\nu} \tag{2}$$

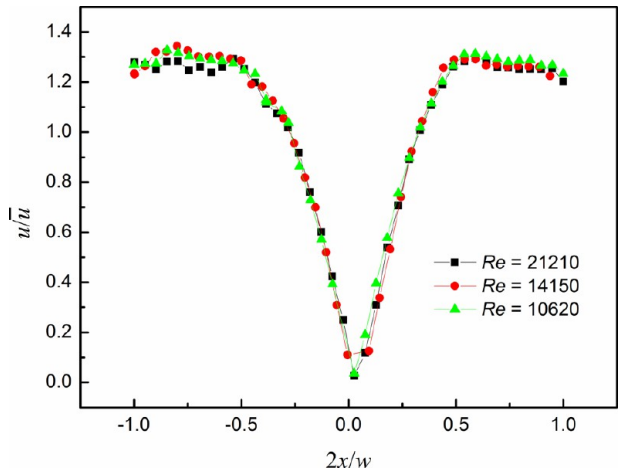

Figure 5. Normalized mean velocity profiles at z = 0 on the $x-z$ plane at three Reynolds numbers (Re = 10 620, 14 150, and 21 210).

where u_i and ν are the mean velocity of the jet and the kinematic viscosity of water, respectively.

dx.doi.org/10.1021/ie400891u | Ind. Eng. Chem. Res. 2013, 52, 11779−11786

The expression for TKE is as follows:

$$k = 0.5(\overline{u_x'^2} + \overline{u_y'^2} + \overline{u_z'^2}) \quad (3)$$

where u_x', u_y', and u_z' are the fluctuating velocities in the x-, y-, and z-directions, respectively. Because the velocity perpendicular to the measurement plane cannot be directly measured by using 2D PIV system, a pseudoisotropic assumption, which has been used and verified by previous investigators,[15,19] was used to estimate the distribution of TKE in this work. On the $x-y$ plane, the TKE is calculated by

$$k = 0.75(\overline{u_x'^2} + \overline{u_y'^2}) \quad (4)$$

On the $x-z$ plane, the TKE is calculated by

$$k = 0.75(\overline{u_x'^2} + \overline{u_z'^2}) \quad (5)$$

The pseudoisotropic assumption was tested in our experiments. The three fluctuating velocities along the x-axis can be obtained from the results obtained on the two planes $x-y$ and $x-z$. The two profiles of TKE, calculated using eqs 3 and 5, were compared with each other, and the maximum difference was <10%.

The method of mechanical energy balance adopted by Siddiqui et al.[14] and Mahajan and Kirwan[10] was used to estimate the averaged energy dissipation rate (ε_{avg}) and the Kolmogorov length scale (λ_K) in our CIJRs. The contribution associated with pressure drop was neglected because the pressure drop could not be measured in the present experimental apparatus. When the jet velocity was within the range of 3.54–7.07 m/s, the ε_{avg} varied from 79.7 m^2/s^3 to 635 m^2/s^3, and λ_K from 10.6 μm to 6.3 μm. The values of ε_{avg} and λ_K in our CIJRs

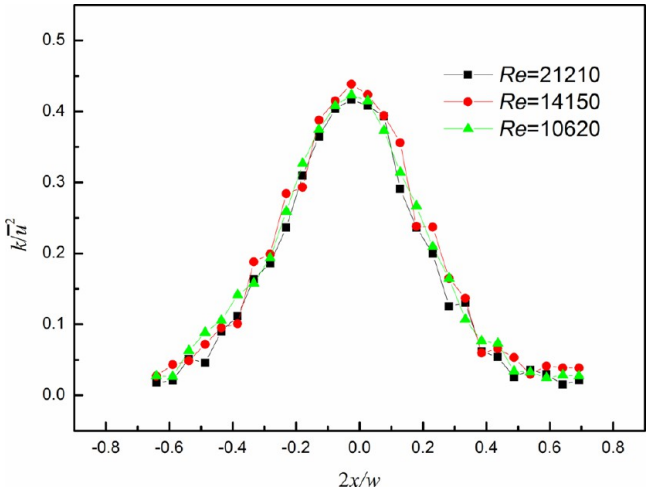

Figure 6. Normalized TKE profiles at $z = 0$ on the $x-z$ plane at three Reynolds numbers (Re = 10 620, 14 150, and 21 210).

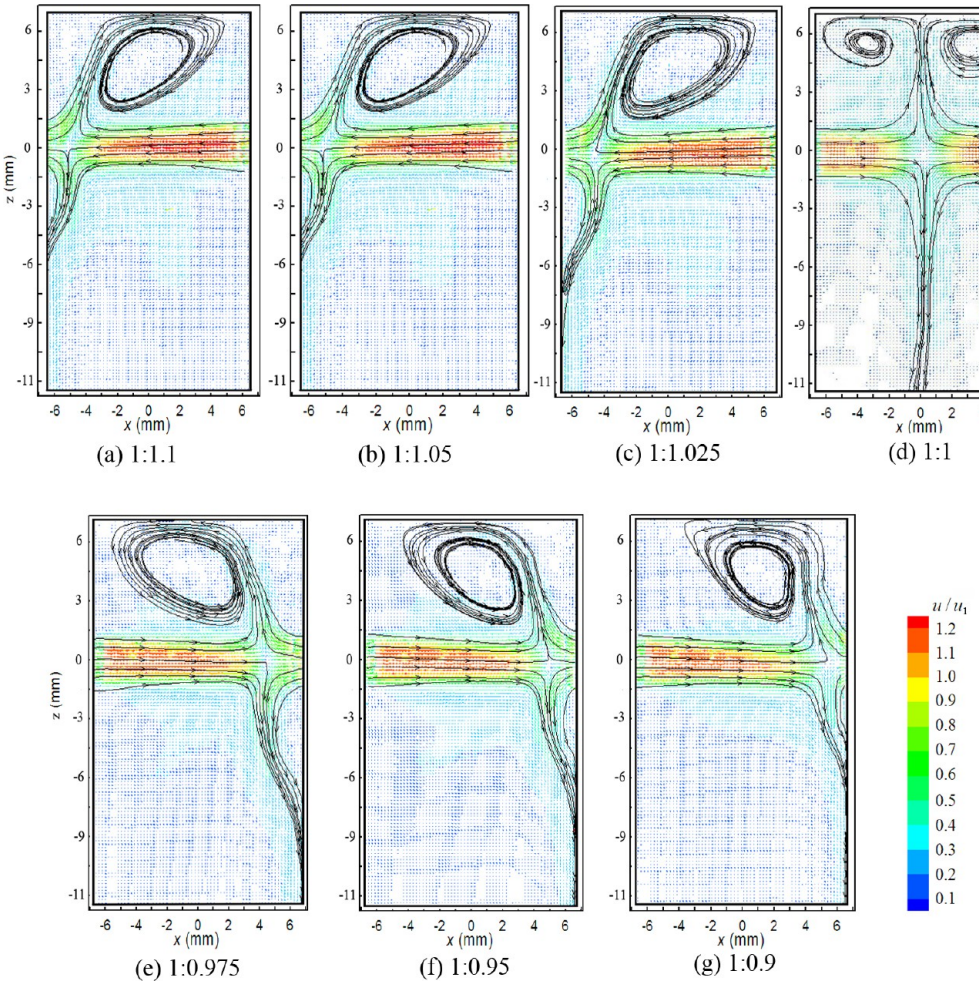

Figure 7. Normalized mean velocity distributions on the $x-z$ plane of CIJR at different jet velocity ratios (u_1/u_2) ($d_1 = d_2 = 3$ mm).

dx.doi.org/10.1021/ie400891u | Ind. Eng. Chem. Res. 2013, 52, 11779–11786

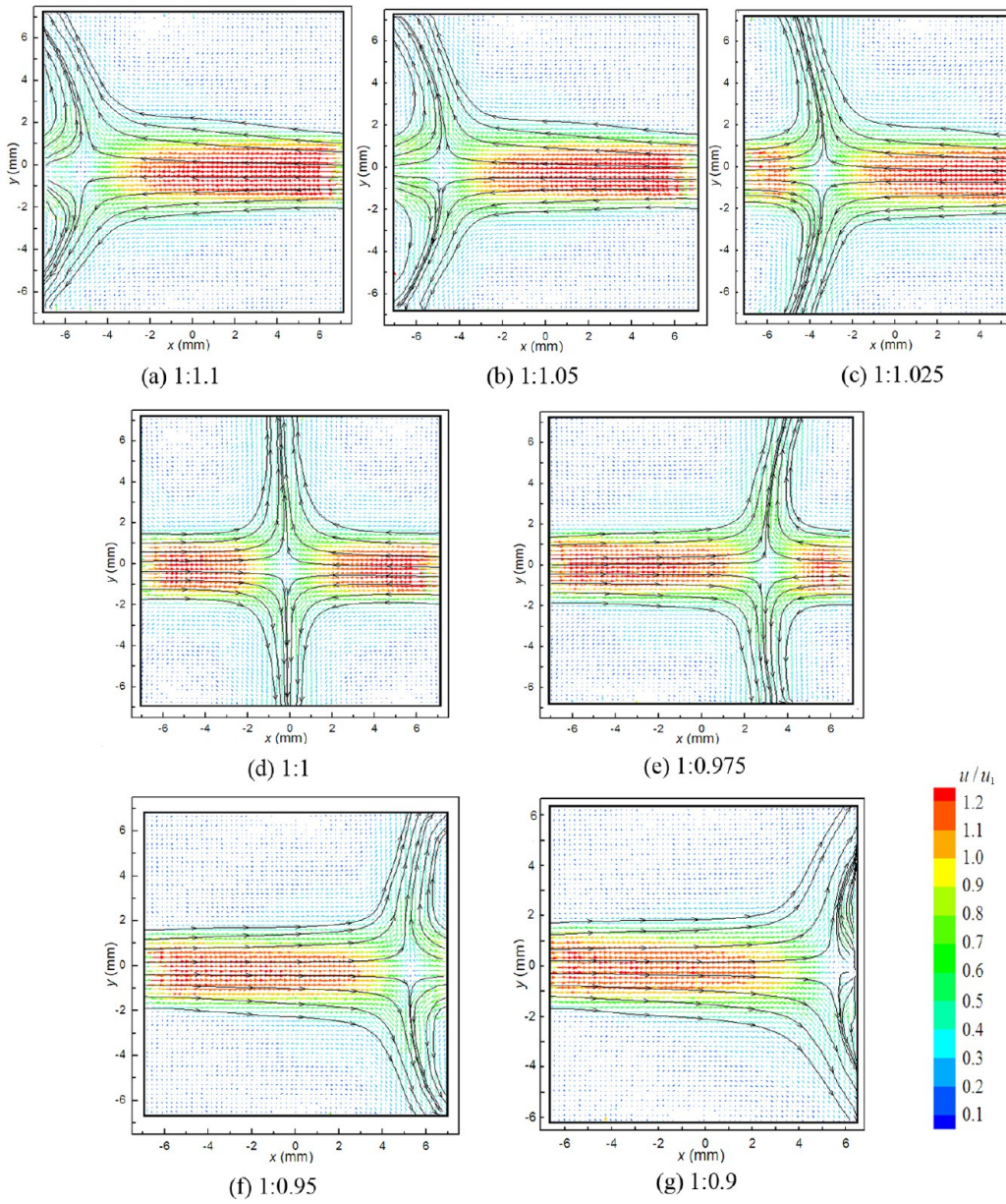

Figure 8. Normalized mean velocity distributions on the $x-y$ plane of CIJR at different jet velocity ratios u_1/u_2 ($d_1 = d_2 = 3$ mm).

are about the same order of magnitude as those in stirred tanks. Thus, the present spatial resolution is sufficient to measure the TKE distributions in CIJRs.

2.3. Operating Conditions. The operating conditions for the CIJRs are listed in Table 1. The experiments were divided into three groups. Group 1 was used to validate the similarity of the turbulent flows at high Reynolds numbers in CIJRs. Group 2 was used to investigate the offset of stagnation points for different diameters of jets when the ratio of the mean jet velocities (u_1/u_2) deviated from 1.0. Group 3 was used to evaluate the effect of the key factor L on the flow pattern of the CIJRs. The chambers of all CIJRs were totally filled with water to avoid the existence of bubbles, which would adversely affect the PIV experiments.

3. RESULTS AND DISCUSSION

3.1. Instantaneous Flow Field. Further to the published studies on the flow fields in CIJRs at low Reynolds numbers ranging from $Re = 60$ to $Re = 2700$,[15,16,20] we investigated the flow characteristics in CIJRs at high Reynolds numbers ($Re = 10\,620$, $14\,150$, and $21\,210$) for the first time. Four instantaneous flow fields on the $x-z$ plane of a CIJR at $Re = 21\,210$ are shown in Figure 3. Detailed flow patterns, eddy structures, and stagnation point offset can be observed, but it is not clear from where they originate.

Flow oscillations and instabilities in CIJRs have been reported by several researchers.[15,16,21] One possible reason for their occurrences is that the flow transitioned from laminar to turbulent in these CIJRs at $Re < 1500$. Another reason may be that gear pumps were used to provide the inflows of the CIJRs. Syringe pumps were used recently in the measurements of a rectangular CIJR to avoid flow oscillations and instabilities.[18]

The flow fields in our CIJRs were fully turbulent at the Reynolds numbers ranging from $Re = 10\,620$ to $Re = 21\,210$. Centrifugal pumps instead of positive displacement pumps such

dx.doi.org/10.1021/ie400891u | Ind. Eng. Chem. Res. 2013, 52, 11779−11786

as gear pumps were used to provide the inflows of our impinging jets. Accurate rotameters with relative errors of <2% were used. The CIJRs and other devices such as pumps and rotameters were installed on separate platforms to minimize the effect of vibration on the CIJRs. The impinging jets of our CIJRs were manufactured using the spark erosion wire cutting technique to guarantee the coaxiality of the two jets in each CIJR.

Therefore, we consider that the variations of the instantaneous flow pattern and stagnation point (see Figure 3) in the present experiments are solely related to the turbulent characteristics in the chamber of the CIJRs. The instantaneous stagnation points in each experiment operated at $u_1/u_2 = 1.0$ were also statistically computed, and over 90% of them were located in the region near the origin ($-0.2 < 2x/w < 0.2$), and none of them deviated from the region $-0.4 < 2x/w < 0.4$.

3.2. Mean Velocity and TKE. Figure 4 shows the normalized mean velocity and TKE distributions on the $x-z$ plane of CIJRs at $u_1/u_2 = 1.0$. The profiles of the normalized mean velocity and TKE at $z = 0$ on the plane are shown in Figures 5 and 6, respectively. The normalized turbulent flow fields at three different Reynolds numbers are similar; that is, the Reynolds number has almost no influence on the normalized velocity and TKE distributions. This result is useful for the design and optimization of CIJRs in industrial applications.

Figure 4 also illustrates the typical flow characteristics of CIJRs. In the impinging region, the mean velocity magnitudes decrease sharply, and the velocity magnitude at the stagnation point is nearly zero. Thus, V-shaped profiles of normalized mean velocities can be seen in Figure 5. However, the TKE values increase rapidly in this region, and the peak value of TKE is located in the vicinity of the stagnation point (see Figure 6). Thus, CIJR is suitable for rapid chemical reaction processes, because the strong collision in CIJR can improve the turbulent mixing efficiency and intensify the transfer between reactants.

3.3. Relationship between Stagnation Point and Jet Velocity Ratio (u_1/u_2). The location of the stagnation point is an important factor in the design and operation of the CIJR. Figures 7 and 8 show the normalized mean velocity distributions at different jet velocity ratios u_1/u_2 on the $x-z$ and $x-y$ planes, respectively (u_1 = 7.86 m/s). The profiles of normalized mean velocity at different jet velocity ratios u_1/u_2 are shown in Figure 9. The flow patterns of the two jets are almost symmetric along the plane $x = 0$ on the two measurement planes when the ratio u_1/u_2 is equal to 1.0 (see Figures 7d and 8d). However, the stagnation point shifts dramatically toward the side wall of the CIJR when the ratio deviates slightly from 1.0. Therefore, accurate and equal volumetric flow rates of the two jets must be maintained for long-term stable operations of the CIJR in industrial applications. Otherwise, the stagnation point may severely deviate from the chamber center, and unexpected backmixing and the formation of byproducts may occur.

Figure 10 quantitatively shows the stagnation point offset Δx at different jet velocity ratios together with error bars. The position of stagnation point is very sensitive to the jet velocity ratio u_1/u_2, and a deviation of only 5% of the ratio can cause a normalized offset of at least 70% along the x-axis. The profiles of the stagnation points on the $x-z$ and $x-y$ planes are very similar; that is, this offset pattern occurs in all three-dimensional (3D) flow fields. With further increase of the deviation of the ratio, the stagnation point is very close to the outlet of the jet with low inlet velocity, and the normalized offset changes slowly. This sensitivity may be due to the complex inelastic collision between the two impinging jets and the change in their kinetic energy. For example, as the mean velocity ratio u_1/u_2 changes from 1.0 to 0.95, the kinetic

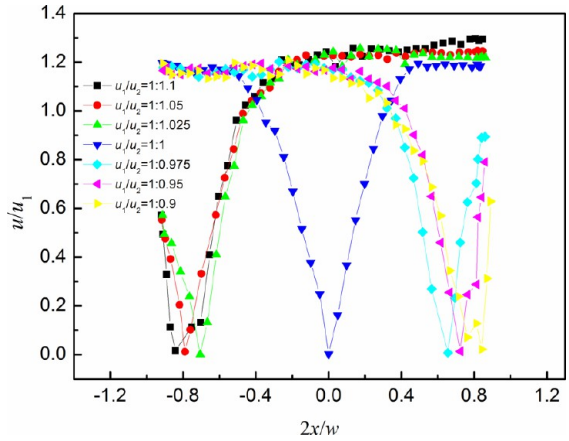

Figure 9. Normalized mean axial velocity profiles at $z = 0$ on the $x-z$ plane of CIJR at different jet velocity ratios u_1/u_2 ($d_1 = d_2 = 3$ mm).

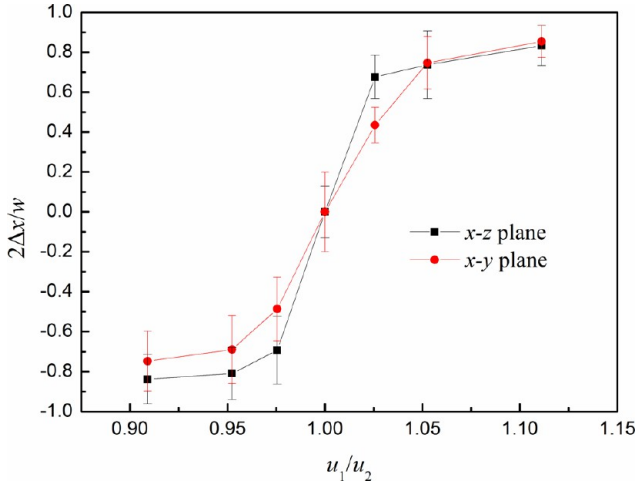

Figure 10. Stagnation point offset on $x-z$ and $x-y$ planes of CIJR at different jet velocity ratios u_1/u_2 ($d_1 = d_2 = 3$ mm).

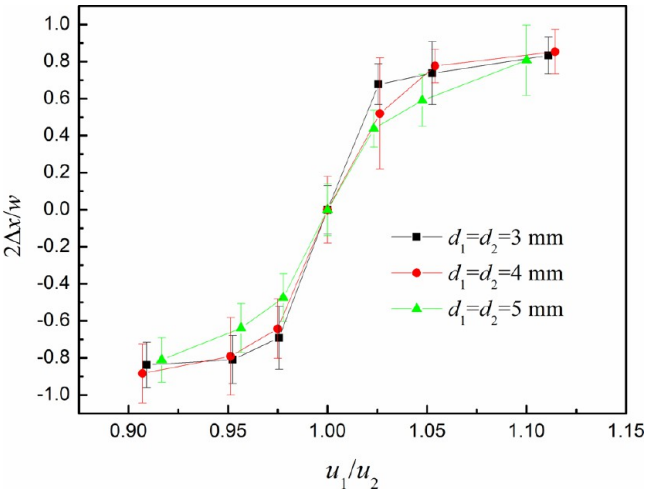

Figure 11. Stagnation point offset on the $x-z$ plane of CIJRs at different jet velocity ratios (u_1/u_2) and jet diameters.

dx.doi.org/10.1021/ie400891u | Ind. Eng. Chem. Res. 2013, 52, 11779−11786

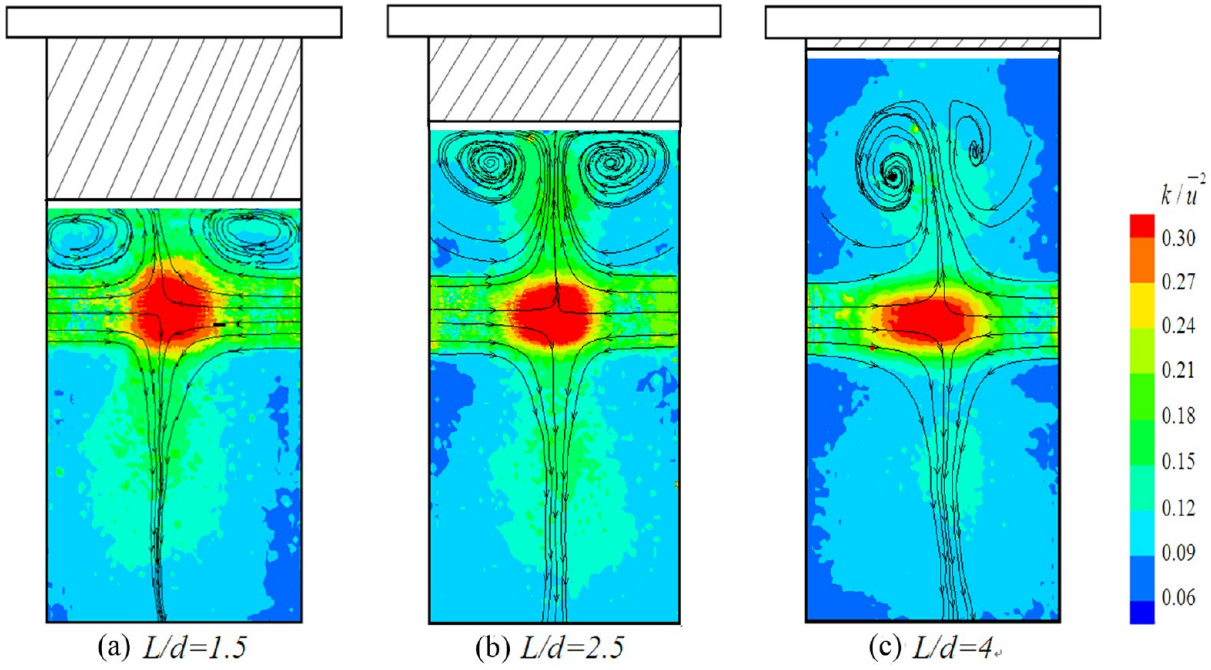

Figure 12. Normalized TKE distributions on the $x-z$ plane of CIJRs with different factors L ($d_1 = d_2 = 3$ mm).

energy ratio $m_1u_1^2/\ m_2u_2^2$ varies from 1.0 to 0.857. This sensitivity was also observed by Li et al.[22] and Sun et al.[23] in their opposed gas jets. Figure 11 presents the effect of jet diameter on the stagnation point offset together with error bars. The stagnation points at different jet diameters shift in a similar range. An increase in jet diameter from 3 mm to 5 mm does not have obvious influence on the offset profiles. Thus, we conclude that the stagnation point offsets are similar for CIJRs with different jet diameters, and this similarity is helpful for the design and operation of CIJRs.

3.4. Effect of Factor *L* on TKE. To investigate the effect of the distance L between the axes of the two jets and the top wall of the CIJR chamber on TKE, the following experimental conditions on the $x-z$ plane in the CIJR were used: Re = 17 670; L/d = 1.5, 2.5, and 4.

Figure 12 shows the normalized TKE distributions of the CIJRs with different factors L/d. The region with high TKE levels ($k/\overline{u}^2 > 0.27$) decreases in size with the increase of L/d from 1.5 to 4. The distribution of the streamlines illustrates that the small spatial dimension above the axes of the two jets restricts the upward development of the impinging streams and makes the streams flow back to the impinging region (see Figure 12a). These complex interactions decrease the rate of mechanical energy transfer from the impinging region to the bulk of the chamber, resulting in the impinging region with high TKE levels, as shown in Figure 12a. On the other hand, the dead region on the top side of the two jets increases in size as L/d increases from 1.5 to 4. That means the more fluid comes into some dead region and keeps low mean and fluctuating velocities, which cannot intensify transfer process. We thus conclude that the decrease of L/d from 4 to 1.5 in the CIJR can increase TKE and enhance the mixing efficiency in the impinging zone, which is beneficial for the mixing of fluids. To summarize, the factor L of a CIJR is also an important parameter for the design of CIJRs, and an optimized L can intensify turbulence transfer and enhance the mixing efficiency of CIJRs.

4. CONCLUSIONS

Normalized mean velocity, turbulent kinetic energy (TKE), and stagnation point offset of confined impinging jet reactors (CIJRs) with various geometric parameters and operating conditions were investigated, using a two-dimensional (2D) particle image velocimetry (PIV) system with high resolution. The effects of Reynolds number, jet velocity ratio, jet diameter, and the key factor L on the flow characteristics of the CIJRs were discussed in detail. In the Reynolds number range of Re = 10 620–21 210, Reynolds number has almost no influence on the normalized velocity and TKE distributions in the CIJRs. The normalized stagnation point offset is very sensitive to the jet velocity ratio, and a 5% change in the ratio can cause at least a 70% offset along the x-axis. Thus, accurate and equal volumetric flow rates of two jets must be used to keep the stagnation point at the center of CIJRs. The region with high TKE levels decreases in size as the L/d value increases from 1.5 to 4. Stable operating conditions and optimized geometric parameters can intensify the turbulence transfer and enhance the mixing efficiency of CIJRs.

AUTHOR INFORMATION

Corresponding Author

*Tel.: +86-10-6441-8267. Fax: +86-10-6444-9862. E-mail: lizp@mail.buct.edu.cn.

Notes

The authors declare no competing financial interest.

ACKNOWLEDGMENTS

The financial supports from the National Natural Science Foundation of China (Nos. 21206002, 21121064, and 20990224) and the State Key Laboratory of Chemical Engineering (No. SKL-ChE-13A03) are gratefully acknowledged.

NOMENCLATURE

d_i = inner diameter of jet (mm)
k = turbulent kinetic energy (m^2/s^2)

L = distance between axes of two jets and top wall of the chamber (mm)
m_i = mass flow of jet (kg/s)
Q_i = volumetric flow rate (m^3/s)
Re = Reynolds number
u = mean velocity magnitude on measurement plane (m/s)
u_i = mean velocity magnitudes of two impinging jets (m/s)
$\overline{u}$ = average velocity of two impinging jets (m/s)
u_x' = fluctuating velocity in the x-direction (m/s)
u_y' = fluctuating velocity in the y-direction (m/s)
u_z' = fluctuating velocity in the z-direction (m/s)
w = width of chamber of CIJR (mm)

Greek Letters

λ_K = Kolmogorov length scale (m)
ν = kinematic viscosity (m^2/s)
ε_{avg} = averaged energy dissipation rate (m^2/s^3)
Δt = time difference between laser pulses (s)
Δx = stagnation point offset along the x-axis (mm)

REFERENCES

(1) Kleingeld, A. W.; Lorenzen, L.; Botes, F. G. The development and modeling of high-intensity impinging stream jet reactors for effective mass transfer in heterogeneous systems. *Chem. Eng. Sci.* **1999**, *54*, 4991−4995.
(2) Hosseinalipour, S. M.; Mujumdar, A. S. Superheated steam drying of a single particle in an impinging stream dryer. *Dry. Technol.* **1995**, *13*, 1279−1303.
(3) Saien, J.; Zonouzian, S. A. E.; Dehkordi, A. M. Investigation of a two impinging-jets contacting device for liquid−liquid extraction processes. *Chem. Eng. Sci.* **2006**, *61*, 3942−3950.
(4) Unger, D. R.; Muzzio, F. J.; Brodkey, R. S. Experimental and numerical characterization of viscous flow and mixing in an impinging jet contactor. *Can. J. Chem. Eng.* **1998**, *76*, 546−555.
(5) Devahastin, S.; Mujumdar, A. S. A numerical study of flow and mixing characteristics of laminar confined impinging streams. *Chem. Eng. J.* **2002**, *85*, 215−223.
(6) Devahastin, S.; Mujumdar, A. S. A numerical study of mixing in a novel impinging stream in-line mixer. *Chem. Eng. Process.* **2001**, *40*, 459−470.
(7) Devahastin, S.; Mujumdar, A. S. A study of turbulent mixing of confined impinging streams using a new composite turbulence model. *Ind. Eng. Chem. Res.* **2001**, *40*, 4998−5004.
(8) Dehkordi, A. M. Novel type of two-impinging-jets reactor for solid-liquid enzyme reactions. *AIChE J.* **2006**, *52*, 692−704.
(9) Hacherl, J. M.; Paul, E. L.; Buettner, H. M. Investigation of impinging-jet crystallization with a calcium oxalate model system. *AIChE J.* **2003**, *49*, 2352−2362.
(10) Mahajan, A. J.; Kirwan, D. J. Micromixing effects in a two-impinging-jets precipitator. *AIChE J.* **1996**, *42*, 1801−1814.
(11) Johnson, B. K.; Prud'homme, R. K. Chemical processing and micromixing in confined impinging jets. *AIChE J.* **2003**, *49*, 2264−2282.
(12) Liu, Y.; Fox, R. O. CFD predictions for chemical processing in a confined impinging-jets reactor. *AIChE J.* **2006**, *52*, 731−744.
(13) Gavi, E.; Marchisio, D. L.; Barresi, A. A. CFD modeling and scale-up of confined impinging jet reactors. *Chem. Eng. Sci.* **2007**, *62*, 2228−2241.
(14) Siddiqui, S. W.; Zhao, Y.; Kukukova, A.; Kresta, S. M. Characteristics of a confined impinging jet reactor: energy dissipation, homogeneous and heterogeneous reaction products, and effect of unequal flow. *Ind. Eng. Chem. Res.* **2009**, *48*, 7945−7958.
(15) Liu, Y.; Olsen, M. G.; Fox, R. O. Turbulence in a microscale planar confined impinging-jets reactor. *Lab Chip* **2009**, *9*, 1110−1118.
(16) Icardi, M.; Gavi, E.; Marchisio, D. L.; Barresi, A. A.; Olsen, M. G.; Fox, R. O.; Lakehal, D. Investigation of the flow field in a three-dimensional confined impinging jets reactor by means of microPIV and DNS. *Chem. Eng. J.* **2011**, *166*, 294−305.
(17) Prasad, A. K.; Adrian, R. J.; Landreth, C. C.; Offutt, P. W. Effect of resolution on the speed and accuracy of particle image velocimetry interrogation. *Exp. Fluids* **1992**, *13*, 105−116.
(18) Somashekar, V.; Liu, Y.; Fox, R. O.; Olsen, M. G. Turbulence measurements in a rectangular mesoscale confined impinging jets reactor. *Exp. Fluids* **2012**, *53*, 1929−1941.
(19) Gavi, E.; Marchisio, D. L.; Barresi, A. A.; Olsen, M. G.; Fox, R. O. Turbulent precipitation in micromixers: CFD simulation and flow field validation. *Chem. Eng. Res. Des.* **2010**, *88*, 1182−1193.
(20) Marchisio, D. L. Large eddy simulation of mixing and reaction in confined impinging jets reactor. *Comput. Chem. Eng.* **2009**, *33*, 408−420.
(21) Icardi, M.; Gavi, E.; Marchisio, D. L.; Olsen, M. G.; Fox, R. O.; Lakehal, D. Validation of LES predictions for turbulent flow in a Confined Impinging Jets Reactor. *Appl. Math. Model.* **2011**, *35*, 1591−1602.
(22) Li, W. F.; Yao, T. L.; Wang, F. C. Study on factors influencing stagnation point offset of turbulent opposed jets. *AIChE J.* **2010**, *56*, 2513−2522.
(23) Sun, Z. G.; Li, W. F.; Liu, H. F. Stagnation point offset of two opposed jets. *Ind. Eng. Chem. Res.* **2010**, *49*, 5877−5883.